

Numerical insights on the structural assessment of historical masonry stellar vaults: the case of Santa Maria del Monte in Cagliari

N. Grillanda · A. Chiozzi · F. Bondi · A. Tralli ·

F. Manconi · F. Stochino · A. Cazzani *

Received: date / Accepted: date

1 **Abstract** The aim of this paper is to present an in-depth numerical investigation on the
2 statics of historical masonry stellar vaults, a special class of masonry ribbed vaults whose
3 three-dimensional geometry features a star-shaped projection on the horizontal plane. In par-
4 ticular, the mechanical behavior of the masonry stellar vault belonging to the church of Santa
5 Maria del Monte in Cagliari (Italy) is analyzed and illustrated as an especially meaningful

* Corresponding author

N. Grillanda

Department of Architecture, Built Environment and Construction Engineering (A.B.C.), Technical University of Milan, Piazza Leonardo da Vinci 32, 20133 Milan, Italy E-mail: grlncl@unife.it

F. Bondi, A. Chiozzi, A. Tralli

Department of Engineering, University of Ferrara, Via Saragat 1, 44122 Ferrara, Italy E-mail: francescobondi.fe@gmail.com , E-mail: chzndr@unife.it , E-mail: tra@unife.it ,

F. Manconi, F. Stochino, A. Cazzani

Department of Civil and Environmental Engineering and Architecture, University of Cagliari, Via Marengo 2, 09123 Cagliari, Italy E-mail: fabio.manconi@gmail.com , E-mail: fstochino@unica.it , E-mail: antonio.cazzani@unica.it ,

6 case study. This church, which was built during the second half of the 16-th century, is a
7 beautiful example of Gothic-Catalan style and its ribbed stellar vault is one of the most rep-
8 resentative of this type in the town of Cagliari. The geometrical outline of the vault has been
9 obtained through laser scanning techniques and a procedure of *reverse engineering*. Starting
10 from a three-dimensional representation of its geometry, the ultimate load bearing capacity
11 of the stellar vault can be accurately estimated through a recently developed, NURBS-based
12 upper bound limit analysis scheme. A comparison with incremental non-linear analyses car-
13 ried out with the commercial finite element code DIANA is presented. Furthermore, the
14 paper also includes a sensitivity study aimed at investigating the role of ribs on the ultimate
15 load bearing capacity of the structure.

16 **Keywords** Historical masonry vaults · stellar vaults · GA-NURBS limit analysis · finite
17 elements · incremental non-linear analysis

18 1 Introduction

19 A stellar vault is a specific kind of Gothic ribbed vaults. It can be considered as an evolution
20 of the traditional cross vault, characterized by a more complex geometry and by a system
21 of supporting ribs. The name is due to the particular shape of its projection on a horizon-
22 tal plane, which usually looks like a star (Kulig and Romaniak, 2007). Stellar vaults have
23 been spread in the Mediterranean area between the 14-th and the 17-th century with the
24 late-Gothic architecture. Several examples of this typology can be found in Sardinia, where
25 stellar vaults are often used as ceilings for the presbytery, namely the most important area
26 of the church. These structures can be considered among the most important works in the
27 history of architecture and constitute a precious masterpiece of the cultural heritage that de-
28 serves being protected. However, their preservation requires a thorough knowledge of many

29 perspectives, starting from constructive ones up to their structural behavior. Gothic builders
30 made great progress in the structural field, with the continuous search for optimal solutions,
31 the progressive reduction of masses and the attempts to differentiate the static role of the
32 various elements of the construction.

33 The structural behavior of Gothic vaults has been the subject of scientific debate for
34 a long time (Huerta Fernández, 2009): in this field different theories have been proposed
35 explaining the structural role of ribs in cross vaults (Di Pasquale, 1996), (Viollet-le-Duc,
36 1854–1868), (Abraham, 1934), (Sabouret, 1928). Because of the lack of specific methods
37 of analysis, the static behavior of such structures is still unclear. In addition to the typical
38 problems of historical masonry building modelling, in this case further difficulties arise, due
39 to the complexity of geometry and the intrinsically three-dimensional character of the prob-
40 lem. The considerable progress recently achieved by numerical modeling techniques, based
41 on the finite element method, and the possibility of producing accurate geometric surveys
42 thanks to laser scanning techniques, make the static behavior of the complex masonry vault
43 an interesting topic of research.

44 In this work an investigation on the structural behavior of masonry stellar vaults is pro-
45 posed: attention is focused on a case study, namely the stellar vault of the church of Santa
46 Maria del Monte in Cagliari, Italy (Freddi and Salinas, 1959), which was built in the second
47 half of the 16-th century in a Gothic-Catalan style (Manconi, 2015). A series of investi-
48 gations about this vault have been performed by laser scanning techniques in combination
49 with a *reverse engineering* procedure. A similar application of laser scanner techniques on
50 the evaluation of the geometry of historical masonry buildings can be found in (Carini and
51 Genna, 2012). The geometric outline has allowed the reconstruction of three-dimensional
52 models in a CAD environment. Mechanical parameters of masonry have been deduced
53 through a series of *in situ* experimental tests and by adopting the prescriptions provided

54 by the Italian Building codes (NTC 2008, 2008), (Circolare n. 617, 2009). As it is well
55 known, the strong heterogeneity of mechanical characteristics of masonry, which includes
56 a very low tensile strength in comparison with a relatively high resistance in compression,
57 makes linear elastic approaches unsuitable (Heyman, 1995), (Como, 2013). Therefore, in
58 this work the structural behavior of this stellar vault has been studied through incremental
59 non-linear analyses and limit analysis.

60 Incremental non-linear analyses have been performed through the FEM-based software
61 DIANA (DIANA, 2015). Different constitutive laws for masonry behavior in tension have
62 been considered. Recently, similar non-linear analyses have been performed on geometri-
63 cally complex ribbed masonry vaults in order to evaluate the structural safety in terms of
64 vertical load (Compán et al., 2017).

65 Limit analysis is the best alternative to non-linear incremental analyses for the eval-
66 uation of the ultimate load bearing capacity of masonry vaults. In the last years different
67 methods have been applied to the study of Gothic vaults: among others, a limit analysis
68 based on a lower-bound approach, which is the so-called Thrust Network Method (Block
69 and Ochsendorf, 2007), (Block and Lachauer, 2014), and techniques based on the Discrete
70 Element Method (Lengyel, 2017). Other approaches based on the upper-bound theorem have
71 been adopted in the study of seismic vulnerability of cross vaults (Gaetani et al., 2017). How-
72 ever, in these latter methods different possible collapse mechanisms must be considered in
73 order to avoid an excessive overestimation of the collapse load multiplier. In this paper a
74 new approach recently proposed in (Chiozzi et al., 2016b), (Chiozzi et al., 2017a), (Chiozzi
75 et al., 2017b), (Chiozzi et al., 2018a), (Chiozzi et al., 2018b) has been applied to the limit
76 analysis of stellar vaults: this procedure is based on the use of a NURBS (Not Rational
77 Uniform B-Spline) model for the representation of the geometry, an upper-bound approach
78 and a genetic algorithm. The use of NURBS surfaces instead of finite elements allows the

79 representation of the exact geometry of the stellar vaults with few elements. Finally, the col-
80 lapse mechanism associated to the minimum load multiplier is determined using a genetic
81 algorithm.

82 It has to be noticed that, despite of its simplicity, Heyman's model may be inappropriate
83 for vaults with the role of roofing elements, which are often characterized by high values of
84 the span-to-thickness ratio and by the absence of backfill: the reader is referred to (Ramaglia
85 et al., 2016) for a detailed research on the most suitable approaches for slender vaults. For
86 these reasons, in the aforementioned model, a non-zero tensile strength and a finite com-
87 pressive strength has been assumed for masonry.

88 The paper is organized as follows. Section 2 contains some historical details about ribbed
89 stellar vaults. Section 3 includes a description of Santa Maria del Monte stellar vault and
90 of the procedure which allowed to obtain the 3D models from the geometric outline of the
91 structure. **Finally, in Section 4 the details of the performed numerical analyses are presented,**
92 **along with a thorough discussion of the obtained results.** In the same Section also a sensitiv-
93 ity analysis of the ultimate load bearing capacity of the vault as a function of ribs' thickness
94 is included. Finally, conclusions are drawn in Section 5.

95 **2 Stellar vaults: generalities**

96 During the late-Gothic period of 13-th and 14-th centuries, different compositions of ribbed
97 cross vaults have been experimented by architects and builders. Through realization of more
98 decorates and complex versions, stellar vaults (i.e. star-shaped vaults) appeared, in which
99 secondary ribs were added to further subdivide the span. These particular vaults owe their
100 name to the projection on the horizontal plane of the ribs system, which is usually a star-
101 shaped figure.

102 The additional elements can be distinguished in main (*tiercerons*) and secondary ribs
103 (*liernes*), respectively ribs which start from the base of the vault and others which have
104 the role of connections. On the horizontal plane, usually star-shaped vault's pattern can be
105 obtained by subdividing the angle into four equal parts (Fig. 1(a)); therefore, main addi-
106 tional ribs are directed along the bisector between projections of perimeter and diagonal
107 arches. A simple graphic method based on the circumscribed circle of the map and the two
108 symmetry axes can be used to define main ribs on the horizontal plane (Casu, 2013) (see
109 Fig. 1(b)). Through the addition of secondary ribs, different geometric shape can be obtained
110 (Fig. 1(c)). Generally, pendulous buds are located under ribs intersections as decorations.

111 The first stellar vaults have been found in France: one of the most meaningful case is lo-
112 cated in the Amiens cathedral (1220-1269) between the central nave and the transept (Willis,
113 1842), (Fitchen, 1961), (Bechmann, 1981). During the late-Gothic period this type has been
114 spread in the Mediterranean and especially in Spain; moreover several cases are located in
115 Poland and Hungary (Kulig and Romaniak, 2007), (Ther et al., 2010). In Sardinia the late-
116 Gothic building typology appeared in the 14-th century with the greatest diffusion between
117 the 15-th and the 17-th (see Fig. 2). Here, under the Crown of Aragona (1324–1479) and the
118 Spanish Kingdom (1479–1714), the development of Gothic culture allowed the comparison
119 of repeatable codified forms, which were used in both civil and religious architecture. Six
120 cases of stellar vaults observed in Cagliari are shown in Fig. 3. As a representative case
121 of this particular type, a detailed analysis of the stellar vault of church of Santa Maria del
122 Monte is presented here.

123 Design, construction and measurement practical techniques on Gothic structures have
124 been described for the first time in the *Portraiture book* or *Livre de portraiture* by Villard de
125 Honnecourt (Lassus, 1858), that is composed by a series of boards compiled approximately
126 in 1230 of which only 66 survived until now. The manuscript is an important proof of role

127 and experience for specialists who lived in that historical period. Rules about building are
128 the main topic developed in the book: about the design of vaults, the so-called three arches
129 rule has been reported, as demonstration of the use of standard building methods.

130 About the late-Gothic vaults also the Renaissance treatises by Alonso de Vandelvira,
131 Hernàn Ruiz and Rodrigo Gil de Hontañòn, (Huerta Fernández, 2006), are truly important.
132 In addition to other topics, specific references to ribbed cross vaults are contained in these
133 works, not only from the point of view of the design but also from that of estimating the size
134 of the ribs.

135 From these works, it is clear that medieval building techniques were based on geomet-
136 ric rules, which are a direct consequence of structural behavior of masonry buildings. In-
137 deed this method is still considered as a fundamental one in the study of historical masonry
138 buildings and it has been proposed several times by Heyman and Como, (Heyman, 1995),
139 (Como, 2013). Buildings were usually made of cut stone. However sometimes vault's webs
140 were made of bricks, which are lighter and easier to lay, whereas stones were used for ribs
141 only. Otherwise, in secondary cases the vault could be built entirely with bricks with special
142 pieces for the ribs (corner bricks).

143 Like for the case of cross vault, the building of the stellar vaults requires production
144 and laying of centrings near ribs and perimeter arches; at the center of the vault diagonal
145 centrings stand on a pillar which is lifted up to the intersection point (Fig. 4).

146 This technique requires ribs to have adequate dimensions to act as support for vaults;
147 usually, they are contoured and made in two different parts: one which is protruding and
148 another whose top is hidden by the vault, as shown in Fig. 5. Guidelines for estimating the
149 size of the ribs, with relation to the dimension of the vault, are reported in several historical
150 essays. As an example, Breyman (Breyman, 1849) suggested a minimum of 13 cm and of
151 27 cm respectively for the width and the depth of a rib corresponding to a span equal to 5 m.

152 From the historical point of view, the role of ribs in cross vaults was highly discussed
153 during the first half of the 20-th century. An interesting review about this topic has been
154 proposed by Di Pasquale (Di Pasquale, 1996).

155 According to Viollet-le-Duc (Viollet-le-Duc, 1854–1868) ribs work as a sort of elas-
156 tic centrings, made by voussoirs that follow structural adjustments and support masonry
157 above them. Viollet pointed out the difference between building and structure, i.e. filling
158 and supporting elements. The supporting interpretation for ribs, proposed by the French ar-
159 chitect, has been called into question some years later by Abraham (Abraham, 1934) and
160 Sabouret (Sabouret, 1928) who suggested, starting by analyses of the great Gothic cathe-
161 drals which had been severely damaged during World War First, that vaults could sustain
162 themselves even without ribs.

163 The study of static scheme of cross vaults is truly complex (Milani et al., 2014); stress
164 are concentrated along diagonals even without protruding ribs. Maybe this fact was already
165 known by Roman constructors, who used to reinforce cross intersections with arches located
166 at the intrados of the vault. In addition, provided that stones used for ribs have usually better
167 mechanical properties than those used for webs (even because of cutting mode and arrange-
168 ment), this further contribution due to mechanical characteristics of the material should be
169 considered.

170 However, the same static interpretation proposed for diagonal ribs in cross vaults (Como,
171 2013) cannot be applied always to additional ribs introduced, for example, in stellar vaults.

172 **3 The stellar vault of Santa Maria del Monte: description and modeling**

173 The church of Santa Maria del Monte (Freddi and Salinas, 1959) (Fig. 6), which is located in
174 Cagliari in the historic district of Castello, was built in the second half of the 16-th century

175 in a Gothic-Catalan style as the seat of the *Arciconfraternita del Sacro Monte di Pietà*.
176 Several changes and renovations have been applied to the church, which is now used as the
177 headquarter of the *Sovereign Military Order of Malta* (Manconi, 2015) in Sardinia.

178 The church is composed by a single nave without transept and with presbytery in the
179 shape of a chapel (*capilla mayor*). The chapel stood out for the squared plan, tighter than
180 the nave, and especially for the star-shaped vault, with ogive ribs connected by *tiercerons*
181 and *liernes* and with five pendulous buds, Fig. 7(a), typical of the late-Gothic architectural
182 style of Sardinia.

183 The very complex and peculiar geometric scheme of this vault, and the utmost impor-
184 tance of precise geometric data for analyzing these structures, required a survey carried out
185 through laser scanning techniques, Fig. 7(b). The obtained point cloud has subsequently
186 been simplified using a Poisson-disk sampling algorithm (Corsini et al., 2012). In this way
187 the geometric characteristics of the structure have been determined with high accuracy, es-
188 pecially small local imperfections and asymmetry (in comparison with the standard pattern
189 provided by architectural essays) have been precisely detected.

190 Generally speaking, the whole vault does not present large deformations. A greater cure
191 in construction can be noticed in ribs than in the vault webs, especially along diagonals.
192 Projections in the horizontal plane are all straight, however the *tiercerons* scheme is a bit
193 different in comparison with the standard design: indeed, they are not directed along the
194 bisector of the angle described by the ogive and the perimeter arch. Arches can be described
195 generally as circular polycentric, forming, especially along the perimeter, little pronounced
196 lancet arches (see Fig. 7(a)). Faint variations in elevation have been found in the additional
197 ribs.

198 There are several hypotheses to explain these variations. It is reasonable to think that
199 Gothic-Catalan constructors, the so-called *picapedras*, had their personal design procedure,

200 improved over the years and maybe somehow different from the standard method; anyway,
201 a span to rise ratio equal to 2 suggests their will to define lancet arches. Otherwise, another
202 possible explanation lies in the use of existing centrings for the construction of ogive arches,
203 which were therefore adapted to their current needs.

204 Starting from the detected point cloud, a three-dimensional NURBS (non-uniform ratio-
205 nal B-splines) model of the whole vault has been obtained by using a solid modeling soft-
206 ware (Rhinoceros[®]) through a process of *reverse engineering*. The model is composed of
207 NURBS surfaces obtained through a refinement of the point cloud (see Fig. 8). The NURBS
208 model has allowed the realization of a second model, to be used for analyses based on the
209 Finite Element Method (FEM), directly in the CAD environment, in which the stellar vault
210 is represented as a three-dimensional solid. In this latter model also the thickness of each
211 element has been represented, as it can be seen in Fig. 9.

212 Diagonal and perimeter arches start 3.5 m in elevation above the floor and the height
213 of the keystone is about 8 m. The horizontal projection corresponds to a square whose side
214 is 6.3 m. These measures are the result of the adopted (and previously explained) scheme.
215 Further simplifications have been necessarily considered for the ribs: indeed the molded
216 sections have been represented as rectangular ones, see Fig. 10 for the assumed geom-
217 etry. The thickness of the vault webs could not be measured directly, thus according to
218 reference information (Viollet-le-Duc, 1854-1868 (Viollet-le-Duc, 1854-1868); Ungewitter
219 and Mohrmann, 1890 (Ungewitter and Mohrmann, 1890); Breyman, (Breyman, 1849);
220 Como, (Como, 2013)) a thickness of 15 cm has been assumed.

221 The vault has been supposed constrained only at the base according to the hypothesis of
222 very low connection with lateral walls, which are located only on two sides (see Fig. 7(a)).

223 The vault is entirely built with cut stone extracted from local quarries. The vaults'
224 structure appears generally regular with brick-rows orthogonally aligned with the perime-

225 ter arches; joints are actually made with lime mortar and have an average thickness equal
 226 to 2 cm, rib joints are instead thinner, indicating a better quality of construction. Mechanical
 227 characteristics of stones depend on the extraction site or even on the outcrop. A direct mea-
 228 sure of mechanical parameters has not been possible, however technical literature (Cuccuru
 229 et al., 2014) suggests the following average values:

- 230 – specific weight: $\gamma = 22.5 \text{ kN/m}^3$
- 231 – dynamic elastic modulus: $E_d = 17.6 \text{ GPa}$

232 The static elastic modulus of bricks, E_b , has been obtained by the dynamic modulus through
 233 relations taken by known sources (see (Eissa and Kazi, 1988)), which directly provide
 234 Eq. (1):

$$E_b = 0.74E_d - 0.82 \cong 12 \text{ GPa} \quad (1)$$

235 In the same way, an estimate of the value Young's modulus for mortar (Parisi and Augenti,
 236 2012) was obtained. In particular a value equal to $E_m = 280 \text{ MPa}$ has been assumed: it
 237 should be noticed that this is a conservative choice, since it results one of the smallest values
 238 obtained by experimental tests.

239 Then Young's modulus for (homogenized) masonry of ribs, E_r , can be obtained through
 240 Eq. (2) (Como, 2013):

$$E_r = E_m \frac{1 + \frac{s}{h_b}}{\frac{E_m}{E_b} + \frac{s}{h_b}} \quad (2)$$

241 where s and h_b represent the joint and brick thicknesses, respectively. In the present case,
 242 it has been assumed for ribs, where the quality of mortar joints is better, $s = 1 \text{ cm}$ and
 243 $h_b = 25 \text{ cm}$ respectively, which would produce, by Eq (2), $E_r = 4.598 \text{ GPa}$. Similarly for the
 244 homogenized masonry vault's webs, where the quality of mortar joints is worse, the assumed

245 values have been: $s = 2$ cm and $h_b = 25$ cm. As a consequence for Young's modulus a value
246 $E_v = 2.926$ GPa has been obtained, which is in good agreement with values suggested by
247 the Italian technical literature (NTC 2008, 2008), (Circolare n. 617, 2009).

248 Values obtained in this way have been successively corrected with safety coefficients
249 provided by the Italian codes. In particular, (NTC 2008, 2008) suggests mechanical param-
250 eters for each type of masonry, and for squared stones there are the following values:

- 251 – specific weight: $\gamma = 22$ kN/m³
- 252 – elastic modulus: $E = 2400 \div 3200$ MPa

253 In conclusion, based on experimental tests given by literature, suggestions of Italian codes
254 and an *in situ* exam, the following values have been adopted:

- 255 – specific weight: $\gamma = 22$ kN/m³
- 256 – Poisson's coefficient: $\nu = 0.2$
- 257 – Young's modulus for vault's webs masonry: $E_v = 2800$ MPa
- 258 – Young's modulus for ribs masonry: $E_r = 4200$ MPa

259 **4 Description of the numerical analyses performed on the vault**

260 The stellar vault of Santa Maria del Monte has been studied through limit analyses and
261 incremental non-linear analyses in order to evaluate the ultimate load bearing capacity of
262 this structure. Two different load configurations have been considered: uniform vertical load
263 and point vertical load applied at the crown (Fig. 11).

264 Limit analyses have been performed through a new procedure recently developed by
265 the research team of the University of Ferrara: this method, the so-called GA-NURBS limit
266 analysis, works in the MATLAB® environment starting by the NURBS model of the vault.
267 Therefore, the geometry has been defined by means of NURBS surfaces (Piegl and Tiller,

1995) through the Rhinoceros[®] code (McNeel, 2008) (Fig. 12). The use of NURBS is particularly suited for masonry vaults, where equilibrium can be verified provided that the thrust surface is strictly enclosed within the exact outline of the structure (Heyman, 1995).

In commercial CAD packages and free-form surface modelers like Rhinoceros[®] description and computation of complex geometries is performed through B-splines and NURBS approximating functions. NURBS basis functions are built on B-splines basis functions, which are piecewise polynomial functions defined by *knots* (i.e. points in a parametric domain) $\Xi = \{\xi_1, \xi_2, \dots, \xi_{n+p+1}\}$, where p and n denote respectively the polynomial order and the total number of basis functions. Given a set of weights $w_i \in \mathbb{R}$ and the i -th B-spline basis function ($N_{i,p}$), then the NURBS basis function $R_{i,p}$ can be written as follows:

$$R_{i,p}(\xi) = \frac{N_{i,p}(\xi) \cdot w_i}{\sum_{i=1}^n N_{i,p}(\xi) \cdot w_i} \quad (3)$$

A NURBS surface of degree p in the u -direction and q in the v -direction is a parametric surface in the three-dimensional Euclidean space defined as:

$$S(u, v) = \sum_{i=0}^n \sum_{j=0}^m R_{i,j}(u, v) B_{i,j} \quad (4)$$

where $B_{i,j}$ form a bidirectional net of control points. A set of weights $w_{i,j}$ and two separate knot vectors in both u and v directions must be defined. Further details about mathematical formulations of NURBS surfaces can be found in (Piegl and Tiller, 1995), while more general IsoGeometric Analysis (IGA) methods have been recently presented in (Khakalo and Niiranen, 2017), in (Cuomo and Greco, 2018) and in (Yildizdag et al., 2018).

In order to perform the limit analysis, the NURBS model generated in Rhinoceros[®] has been imported into the MATLAB[®] environment through the IGES (Initial Graphic Exchange Specification) standard (Kennicott, 1996). A set consisting of 33 NURBS surfaces

288 has been used: 12 surfaces defining the vault's webs, 20 the ribs and 1 the keystone (see
 289 Fig. 12). The thickness of each of these surfaces has been assigned directly in MATLAB®:
 290 the model obtained in this way is shown in Fig. 13.

291 A NURBS mesh is then defined on this model, where each element of the mesh still
 292 consists of a NURBS surface and, hence, can be regarded as a rigid body. Dissipation,
 293 which is evaluated according to a rigid-plastic behavior in tension, compression and shear,
 294 is allowed only along element edges: therefore, element edges represent potential fracture
 295 lines. In this way the kinematics of each element is determined by six degrees of free-
 296 dom, which are the three translational and three rotational generalized velocity components
 297 $\{u_x^i, u_y^i, u_z^i, \phi_x^i, \phi_y^i, \phi_z^i\}$ of its center of mass G_i , expressed in a global reference system $O_{x,y,z}$.

298 Let us assume that the vault is subjected to two group of loads: *i*) loads which are inde-
 299 pendent of the collapse multiplier λ (say F_0 , e.g. gravity loads, which do not change their
 300 intensity during the loading process) and *ii*) loads which depend on λ (say λT_0 , e.g. vari-
 301 able vertical load, whose intensity changes during the loading process, being incremented
 302 by the multiplier λ ; T_0 is here the so-called unit vector of actions, corresponding to a value
 303 $\lambda = 1$ of the collapse multiplier). A so-called normalization condition, classically obtained
 304 by imposing that power dissipated by loads depending on λ is unit when $\lambda = 1$, is needed
 305 to restrict the homothetic failure mechanism to one. Such normalization condition can be
 306 written as follows:

$$D_{T_0} = \mathbf{T}_0^T \mathbf{U} = 1 \quad (5)$$

307 where \mathbf{U} is the vector of assembled generalized velocities for all the elements. Consequently,
 308 the dissipated external power is the following:

$$D_{ext} = D_{F_0} + \lambda D_{\Gamma_0} = \mathbf{F}_0^T \mathbf{U} + \lambda \quad (6)$$

309 Equating internal, D_{int} , and external dissipation, D_{ext} , in the framework of the upper bound
 310 theorem, where it is required the minimization of λ , the objective function is therefore $\lambda =$
 311 $D_{int} - \mathbf{F}_0^T \mathbf{U}$ and the collapse load multiplier λ does not enter as an independent variable in
 312 the Linear Programming problem.

313 External constraints and boundary conditions on velocities are standard and, after suit-
 314 able assemblage, lead to a set of equalities that can be written in compact notation as follows:

$$\mathbf{A}_{eq,geom} \mathbf{U} = \mathbf{b}_{eq,geom} \quad (7)$$

315 where $\mathbf{A}_{eq,geom}$ is the matrix of geometric constraints and $\mathbf{b}_{eq,geom}$ the corresponding vector
 316 of known coefficients.

317 Plastic compatibility constraints are imposed on interfaces, subdividing edges into N_{sd}
 318 segments and $(N_{sd} + 1)$ collocation points P_i , as sketched in Fig. 14(a). A local frame of
 319 reference $(\mathbf{n}, \mathbf{s}, \mathbf{t})$ on each P_i is easily defined, indicating with \mathbf{n} the unit normal vector to
 320 the interface, with \mathbf{s} the unit tangent vector in the longitudinal direction and with \mathbf{t} the unit
 321 tangent vector in the transversal direction. After a suitable linearization of the failure surface
 322 at P_i the following compatibility equation must hold:

$$\Delta \tilde{\mathbf{u}} = \left(\dot{\lambda}^T \frac{\partial f}{\partial \boldsymbol{\sigma}} \right)^T \quad (8)$$

323 where $\boldsymbol{\sigma} = [\sigma_{n,n}, \tau_{n,s}, \tau_{n,t}]^T$ is the stress vector acting on P_i in the local frame of reference,
 324 $f(\boldsymbol{\sigma})$ is the linearized strength domain ($\partial f / \partial \boldsymbol{\sigma}$ is therefore a three-column matrix of coeffi-
 325 cients of the linearization plane), $\dot{\lambda}$ is the vector of non-negative plastic multiplier rates and
 326 $\Delta \tilde{\mathbf{u}}$ is a 3×1 vector of jump of velocities on P_i written in the local frame of reference.

327 Internal dissipation on a single interface i of area S_i is estimated by numerical integration
 328 at collocation points as follows:

$$D_{int}^i = \int_{S_i} \boldsymbol{\sigma} \cdot \Delta \tilde{\mathbf{u}} dS = \int_{S_i} \dot{\boldsymbol{\lambda}}^T \cdot \left(\boldsymbol{\sigma}^T \frac{\partial f}{\partial \boldsymbol{\sigma}} \right)^T dS = \int_{S_i} \dot{\boldsymbol{\lambda}}^T \cdot \mathbf{b}_{sd} dS \quad (9)$$

329 where \mathbf{b}_{sd} is the column-vector of known coefficients of the strength-domain linearization
 330 planes.

331 The obtained linear programming problem, which is used to estimate the collapse mul-
 332 tiplier via an upper bound approach, is therefore the following:

$$\min\{D_{int}^i - \mathbf{F}_0^T \mathbf{U}\} \quad \text{such that } \{\mathbf{A}^{eq} [\mathbf{U}^T \dot{\boldsymbol{\lambda}}^{assT}] = \mathbf{b}^{eq} \text{ and } \dot{\boldsymbol{\lambda}}^{assT} \geq 0\} \quad (10)$$

333 where \mathbf{A}^{eq} is the overall equality constraints matrix (and \mathbf{b}^{eq} the corresponding right-hand-
 334 side vector) collecting plastic flow constraints on discontinuities, velocity boundary condi-
 335 tions and external power normalization condition and $\dot{\boldsymbol{\lambda}}^{assT}$ is the assembled vector of plas-
 336 tic multiplier rates. The solution of the linear programming is found through the MATLAB®
 337 toolbox for optimization over symmetric cones SeDuMi (Self-Dual-Minimization, (Sturm,
 338 1999)); the reader is referred to (Milani et al., 2006) for a critical discussion of the most
 339 effective tools to solve such optimization problem efficiently.

340 A Genetic Algorithm (GA) is here used to adjust the mesh in order to find the minimum
 341 collapse multiplier among all possible configurations and therefore to determine the actual
 342 collapse mechanism. GA is a method for solving both constrained and unconstrained op-
 343 timization problems based on a natural selection process that mimics biological evolution.
 344 The algorithm repeatedly modifies a population of individual solutions. At each step, the
 345 genetic algorithm randomly selects individuals from the current population and uses them
 346 as parents to produce the children for the next generation. Over successive generations, the

347 population “evolves” toward an optimal solution. In this way, it is possible to find the posi-
 348 tion of fracture lines associated to the minimum kinematic multiplier, which are the collapse
 349 mechanism and the collapse multiplier.

350 The reader is referred to (Chiozzi et al., 2017b) for further details about the GA-NURBS
 351 limit analysis and to (Chiozzi et al., 2016b), (Chiozzi et al., 2017a), (Chiozzi et al., 2018a),
 352 (Chiozzi et al., 2018b) for previous applications. It should be noticed that this is the natural
 353 evolution of the previously published (Chiozzi et al., 2016a) open-source code ArchNURBS.

354 The above outlined procedure has been applied in the present case to the stellar vault
 355 of Santa Maria del Monte for determining the collapse load corresponding to the two al-
 356 ready considered cases of uniformly distributed vertical load and of point load applied at
 357 the crown. To this purpose, a Mohr-Coulomb failure criterion supplemented by a linear cap
 358 in compression (Milani and Taliercio, 2016) has been applied to interfaces between ma-
 359 sonry elements; the three-dimensional linearized failure surface is shown in Fig. 14(b) and
 360 Fig. 14(c), whereas material parameters adopted in the analyses are reported in Table 1 (see
 361 Fig. 14(b)) for the meaning of the symbols). The collapse loads for the afore-mentioned
 362 loading conditions resulted to be 41.5 kN/m² and 178.8 kN respectively; the corresponding
 363 collapse mechanism are depicted in Fig. 15 and Fig. 16.

364 As it can be seen in Fig. 15(c), the collapse due to the uniformly distributed vertical
 365 load is mainly characterized by crushing of the masonry at the base of the vault (crushing
 366 at the base is highlighted in Fig. 15(a) by observing the position of the deformed vault in
 367 comparison with the initial constraint plane, which is depicted through dashed lines). This
 368 result descends directly from the geometry of the vault: with this load configuration, the
 369 lowered shape of the ogive and the perimeter arches prevent a collapse produced by the
 370 opening of flexural joints typical of semicircular arches. It is clear that in this situation an
 371 accurate estimate of the masonry ultimate compressive strength becomes fundamental for

Table 1 Masonry parameters adopted for the NURBS model.

Property	Symbol	Value	Unit
Specific weight	γ	22	kN/m ³
Ultimate tensile strength	f_t	0	MPa
Cohesion	c	0.1	MPa
Friction angle	Φ	27	°
Ultimate compressive strength	f_c	2.4	MPa
Parameters defining the shape of the linearized compressive capacity	Φ_2	10	°
	ρ	0.5	—

372 reliably evaluating the collapse load. This is not occurring in the case of a concentrated load
 373 applied at the crown: here the opening of flexural joints on the perimeter arches is clearly
 374 visible (see Fig. 16(c)). In this case, ribs have the typical behavior of arches subjected to a
 375 pointed load applied at the midpoint, whereas vault's webs appear to follow arches in the
 376 collapse. However, for both considered load configurations, the supporting function seems
 377 to be mostly provided by ribs.

378 In order to confirm the results obtained with the limit analysis, a series of incremen-
 379 tal non-linear analyses has been conducted on a FEM model of the stellar vault through
 380 the commercial software DIANA (version 10.2) (DIANA, 2015). Starting by the 3D CAD
 381 model, a mesh composed by 29665 tetrahedral finite elements has been obtained (a value of
 382 0.2 m has been assigned as mesh-size). The use of tetrahedral elements (TE12L in DIANA,
 383 characterized by 12 degrees of freedom, Fig. 17) has allowed a more refined discretization
 384 of the complex geometry of the stellar vault in comparison with parallelepiped-shaped el-
 385 ements: the FEM model is shown in Fig. 18. Two different material properties have been
 386 assigned in DIANA to ribs and vault's webs in order to represent correctly the two different
 387 type of previously mentioned masonry. A Total Strain Crack Model (TSCM) has been used

388 for both materials. Two different options have been considered for the tensile behavior: a bi-
 389 linear elastic-softening and an elastic-plastic behavior (in the latter, elastic-plastic behavior,
 390 a very low value for ultimate tensile strength has been adopted in comparison with the value
 391 of peak tensile load in the bilinear one). Despite the fact that it is often considered unsuitable
 392 to model masonry material, an elastic-plastic tensile behavior has been taken into account
 393 in order to yield a more realistic constitutive law than the rigid-plastic behavior adopted in
 394 the limit analysis. An elastic-plastic behavior has been assigned in compression, whereas
 395 for modeling the stress-strain shear behavior, a shear retention factor β is used as a stiffness
 396 correction (by reducing the shear modulus G , which is computed for elastic isotropic con-
 397 ditions as $G = E/[2(1 + \nu)]$) due to progressive material damaging. Masonry behavior in
 398 tension, compression and shear have been reported in Fig. 19 whereas the relevant parameter
 399 data are shown in Table 2.

400 DIANA software is able to model the progress of damage at each load step. With ref-
 401 erence to the two different tensile behavior diagrams adopted, a different type of damage
 402 is related to each branch of the graphs: for clarity's sake a legend is shown in Fig. 20. A
 403 decrease of load has not been provided in this case study; however unloading phases for the
 404 single element are equally possible because of the stress redistribution due to the progressive
 405 damage of the model.

406 In the analysis of the vault under uniform vertical load an initial load of 1 kN/m^2 has
 407 been applied: 200 load steps have been provided with a load increment of 0.5 kN/m^2 for
 408 each step.

409 Ultimate load values corresponding to 39 kN/m^2 and to 48 kN/m^2 have been obtained
 410 respectively for the bilinear and the elastic-plastic behavior in tension. The corresponding
 411 load-deflection diagrams and the observed crack-patterns are shown in Fig. 21 and Fig. 22,
 412 respectively for the two different tension behaviors.

Table 2 Homogenized masonry parameters adopted for the FEM model

Property	Symbol	Value	Unit
Young's modulus for vault's webs	E_v	2800	MPa
Young's modulus for ribs	E_r	4200	MPa
Poisson's coefficient	ν	0.2	—
Specific weight	γ	22	kN/m ³
Ultimate tensile strength for bilinear elastic-softening behavior	f_t	2.4	MPa
Ultimate tensile strain for bilinear elastic-softening behavior	ϵ_u	0.0001	—
Ultimate tensile strength for elastic-plastic behavior	f_t	0.05	MPa
Ultimate compressive strength	f_c	2.4	MPa
Shear retention factor	β	2.4	—

413 It is useful to highlight that all Figures have been drawn by assuming as the reference
 414 configuration for the vault the one due to self-weight. As a consequence, deflection val-
 415 ues produced by the superimposed live load starts from zero, but correspond to an already
 416 stressed configuration, accounting for the effects of self-weight, acting as a dead load.

417 In the analysis of the vault under a concentrated vertical force applied at the crown an
 418 initial force of 1 kN has been applied. Load increments corresponding to 400 load steps have
 419 been provided, with a load increment equal to 1 kN for each step. For this load condition,
 420 ultimate load values corresponding to 144 kN and to 196 kN have been found respectively
 421 for the two different behaviors in tension. The relevant load-deflection diagrams and the
 422 resulting crack-patterns are shown in Fig. 23 and Fig. 24. Previous analyses (performed
 423 with DIANA version 9.5) corresponding to the second load condition only can be found
 424 in (Grillanda et al., 2017), where a comparison between a perfect model and a model with
 425 geometric imperfections have also been shown.

Please cite this document as: N. Grillanda, A. Chiozzi, F. Bondi, A. Tralli, F. Manconi, F. Stochino and A. Cazzani "Numerical insights on the structural assessment of historical masonry stellar vaults: the case of Santa Maria del Monte in Cagliari" Continuum Mechanics and Thermodynamics, Vol 33:1–24, 2021. DOI:10.1007/s00161-019-00752-8

426 A comparison between results obtained through the two procedures is shown in Fig. 25
 427 and Fig. 26, respectively for uniformly distributed and point-concentrated loads. For the lat-
 428 ter load case a higher difference between the ultimate load values can be noticed: it is the
 429 authors' opinion that this is the natural consequence of the representation of a complex col-
 430 lapse mechanism through few rigid elements only, and that a more accurate value could be
 431 obtained by increasing the number of NURBS surface (despite a larger number of variables
 432 and a corresponding increase of computational cost).

433 GA-NURBS limit analysis may be of great advantages in comparison with FEM in-
 434 cremental analyses. First, it allows to obtain good results with very few elements: for the
 435 stellar vault presented here a total number of 73 elements for the distributed load and 113
 436 for the pointed load has been used. Secondly, on this elaborated case study the evaluation of
 437 the load multiplier associated to a specific configuration of fracture lines may take from 10
 438 to 16 seconds. Despite the complexity, the possible collapse mechanism under vertical load
 439 configurations are limited, thus the convergence is usually reached after few generations
 440 even using a small population size: in this way, the whole procedure takes from 14 to 18
 441 minutes. FEM incremental analyses on the stellar vaults took (on the same hardware plat-
 442 form) about 20 minutes, so the computational time of limit analysis is slightly lower. It has
 443 to be noticed that MATLAB® is not the most efficient programming environment; the use of
 444 programming languages based on pre-compiled library could reduce significantly the com-
 445 puting time of GA-NURBS limit analysis. Finally, the latter approach allows modifications
 446 of the final model directly in MATLAB® without resorting to the modeling software.

447 The great ease by which changes may be applied to the NURBS model has allowed to
 448 carry out a sensitivity analysis on ribs thickness through the presented GA-NURBS limit
 449 analysis. The aim of this sensitivity analysis is to inspect the effective contribution provided
 450 by ribs to the global strength of the stellar vault. Thickness values of ribs have been modified

451 in MATLAB® directly and the analysis has been re-executed for each of such values: indeed,
452 the “thickness property” of NURBS surfaces can be changed *ad libitum* and “on the fly” by
453 the user, exactly in the same way as material properties can be modified in commercial FEM
454 software.

455 For this study, only the case of a uniformly distributed vertical load has been considered,
456 because it is more realistic in relation with the position of the vault. Indeed, the vault is part
457 of the roofing of the church, therefore there are no structural elements that may exert point
458 forces; the most plausible variable load condition is represented by snow load, which can be
459 represented by a constant uniform pressure.

460 The ultimate load bearing capacity in terms of a uniformly distributed vertical load has
461 been inspected by making the hypothesis that all ribs have an equal thickness corresponding
462 to 30 cm, 20 cm, 10 cm or 0 cm (this last case corresponds obviously to the case of a rib-
463 less stellar vault, where only vault’s webs can resist to loads). For the sake of simplicity in
464 this case the same cross-section has been assumed for the entire rib system, therefore the
465 thickness value considered for each case has been assigned to both main and secondary ribs.

466 The obtained results are reported in Fig. 27 (where ribs thickness is denoted by s). Sub-
467 stantial differences on the detected collapse mechanisms have not been observed: because
468 of the lowered shape of the vault, crushing of the masonry at the base of the vault remains
469 fundamental for obtaining a collapse mechanism (in the same way as Fig. 15 shows, the
470 dashed lines in Fig. 27 represents the initial constraint plane). The collapse multiplier in-
471 stead decreases considerably, because the crushed portion of masonry varies from case to
472 case. Fig. 28 shows the different obtained collapse loads: it can be noticed that the collapse
473 load of the previously analyzed case (to be considered as “the real one”) is about 4 times
474 larger than the collapse load of the rib-less vault. This sensitivity analysis confirms once
475 more, if the hypothesis of a good connection between ribs and vault’s webs is fulfilled, that

476 the support function provided by ribs is of utmost importance in the overall strength of the
477 stellar vault.

478 **5 Conclusions**

479 The mechanical behavior of historical masonry stellar vaults has been investigated in this
480 paper. In particular, the ultimate behavior under vertical loads of a complex ribbed stellar
481 vaults, which is typical of Gothic architecture, has been studied.

482 The stellar vault of Santa Maria del Monte church in Cagliari (Italy) has been accu-
483 rately measured through laser-scanning techniques and then reconstructed with a three-
484 dimensional NURBS-based model.

485 A recently developed limit analysis approach based on an adaptive NURBS modeling
486 coupled with a genetic algorithm has been performed on the vault. This method, particularly
487 suited for historical masonry vaults characterized by complex geometry, has been used in
488 order to evaluate the ultimate load of the structure and the associated collapse mechanisms
489 for two different load conditions. Limit analysis results have then been compared with load-
490 deflection curves and crack/damage patterns provided by finite element analyses performed
491 with the commercial code DIANA. A good agreement in terms of both ultimate load and
492 collapse mechanism between limit analysis and FEM-based simulations has been noticed.
493 The reduced computational cost and the quick handling of complex models suggest the
494 adoption of the proposed limit analysis method for future analyses on ribbed masonry vaults.

495 As a final test, the influence of rib thickness on the ultimate bearing capacity of the
496 whole vault has been checked through a sensitivity analysis: the obtained results confirm the
497 remarkable strengthening effect produced by ribs and give a useful insight on the evolution
498 of the collapse mechanism for the whole vault. Future research directions following up the

499 results contained in this paper will include the study of new monitoring techniques (as for
500 example (Cabboi et al., 2017)), the influence of horizontal loads (Valluzzi, 2007) and set-
501 tlements (Iannuzzo et al., 2018), and the development of innovative strengthening solutions
502 (see (Garmendia et al., 2014) for applications on masonry arches).

503 Possible extensions of the formulation adopted for the presented problems could encom-
504 pass the use of Cosserat theory, see for instance (Altenbach et al., 2010), (Eremeyev et al.,
505 2015), (Eremeyev and Altenbach, 2017), (Miśkiewicz, 2018) for a more accurate descrip-
506 tion of the behavior of the vault's webs and ribs, and non-standard higher gradient elasticity
507 models like those presented in (Placidi et al., 2016) and in (Andreas et al., 2016) or, within
508 a non-conservative setting, in (Placidi et al., 2018). Finally, inspiration for non-linear FEM
509 analyses might be found in (Chróścielewski et al., 2018) and discrete models which are
510 suitable for large displacement analysis are dealt with in (Turco, 2018).

511 **Acknowledgements** The financial support of Fondazione di Sardegna and R.A.S. (the Autonomous Region
512 of Sardinia) under the research grant for project *Healthy Cities and Smart Territories* (2016–2017) is grate-
513 fully acknowledged by Antonio Cazzani.

514 The financial support of the Autonomous Region of Sardinia under grant PO-FSE 2014–2020, CCI: 2014-
515 IT05SFOP021, Project: *Retrofitting, rehabilitation and requalification of the historical cultural architectural*
516 *heritage (R3-PAS)* is acknowledged by Flavio Stochino.

517 Laser scanning of the stellar vault of Santa Maria del Monte Church has been performed with the equipment
518 of LabMAST (the *Mediterranean Lab for Materials and Historical and Traditional Architectures* belonging
519 to the University of Cagliari) by Monica Deidda and Andrea Dessì. Their professional help is recognized with
520 gratitude by all authors.

521 **References**

522 Abraham P (1934) *Viollet-le-Duc et le rationalisme médiéval* Paris. Vincent et Fréal, Paris

Please cite this document as: N. Grillanda, A. Chiozzi, F. Bondi, A. Tralli, F. Manconi, F. Stochino and A. Cazzani "Numerical insights on the structural assessment of historical masonry stellar vaults: the case of Santa Maria del Monte in Cagliari" Continuum Mechanics and Thermodynamics, Vol 33:1–24, 2021. DOI:10.1007/s00161-019-00752-8

- 523 Altenbach J, Altenbach H, Eremeyev VA (2010) On generalized Cosserat-type theories
524 of plates and shells: a short review and bibliography. *Archive of Applied Mechanics*
525 80(1):73–92
- 526 Andraus U, dell’Isola F, Giorgio I, Placidi L, Lekszycki T, Rizzi NL (2016) Numerical sim-
527 ulations of classical problems in two-dimensional (non) linear second gradient elasticity.
528 *International Journal of Engineering Science* 108:34–50
- 529 Bechmann R (1981) *Les racines des cathédrales: l’architecture Gothique, expression des*
530 *conditions du milieu*. Payot, Paris
- 531 Block P, Lachauer L (2014) Three-Dimensional (3D) equilibrium analysis of gothic masonry
532 vaults. *International Journal of Architectural Heritage* 8:312–335
- 533 Block P, Ochsendorf J (2007) Thrust network analysis: A new methodology for three-
534 dimensional equilibrium. *Journal of the International Association for Shell and Spatial*
535 *Structures* 48:1–7
- 536 Breymann GA (1849) *Allgemeine Bau-Constructions-Lehre mit besonderer Beziehung auf*
537 *das Hochbauwesen — I Theil — Constructionen in Stein*. Hoffmann, Stuttgart
- 538 Cabboi A, Gentile C, Saisi A (2017) From continuous vibration monitoring to FEM-based
539 damage assessment: Application on a stone-masonry tower. *Construction and Building*
540 *Materials* 156:252–265
- 541 Carini A, Genna F (2012) Stability and strength of old masonry vaults under compressive
542 longitudinal loads: Engineering analyses of a case study. *Engineering Structures* 40:218–
543 229
- 544 Casu P (2013) *Late gothic vaults in Sardinia: Design, measure, material*. PhD thesis, Uni-
545 *versity of Cagliari, Italy, (in Italian)*
- 546 Chiozzi A, Malagù M, Tralli A, Cazzani A (2016a) ArchNURBS: NURBS-based tool for
547 the structural safety assessment of masonry arches in MATLAB. *ASCE Journal of Com-*

- 548 puting in *Civil Engineering* 30:#04015010–1–11
- 549 Chiozzi A, Milani G, Grillanda N, Tralli A (2016b) An adaptive procedure for the limit anal-
550 ysis of FRP reinforced masonry vaults and applications. *American Journal of Engineering*
551 and Applied Sciences 9:735–745
- 552 Chiozzi A, Milani G, Grillanda N, Tralli A (2017a) Fast and reliable limit analysis approach
553 for the structural assessment of FRP-reinforced masonry arches. *Key Engineering Mate-*
554 rials 747:196–203
- 555 Chiozzi A, Milani G, Tralli A (2017b) A genetic algorithm NURBS-based new approach for
556 fast kinematic limit analysis of masonry vaults. *Computers & Structures* 182:187–204
- 557 Chiozzi A, Grillanda N, Milani G, Tralli A (2018a) UB-ALMANAC: An adaptive limit anal-
558 ysis NURBS-based program for the automatic assessment of partial failure mechanisms
559 in masonry churches. *Engineering Failure Analysis* 85:201–220
- 560 Chiozzi A, Milani G, Grillanda N, Tralli A (2018b) A fast and general upper-bound limit
561 analysis approach for out-of-plane loaded masonry walls. *Meccanica* 53:1875–1898
- 562 Chróscielewski J, Schmidt R, Eremeyev VA (2018) Nonlinear finite element modeling
563 of vibration control of plane rod-type structural members with integrated piezoelectric
564 patches. *Continuum Mechanics and Thermodynamics* pp 1–42, DOI 10.1007/s00161-
565 018-0672-4
- 566 Circolare n. 617 (2009) Instructions for the application of the new Technical Rules for Con-
567 structions. *Gazzetta Ufficiale* n. 47, February 26, 2009 - Suppl. Ordinario n. 27, (in Italian)
- 568 Como M (2013) *Statics of historic masonry constructions*. Springer, Berlin-Heidelberg
- 569 Compán V, Pachón P, Cámara M, Lourenço PB, Sáez A (2017) Structural safety assess-
570 ment of geometrically complex masonry vaults by non-linear analysis. the Chapel of the
571 Würzburg Residence (Germany). *Engineering Structures* 140:1–13

- 572 Corsini M, Cignoni P, Scopigno R (2012) Efficient and flexible sampling with blue noise
573 properties of triangular meshes. *IEEE Transactions on Visualization and Computer*
574 *Graphics* 18:914–924
- 575 Cuccuru F, Fais S, Ligas P (2014) Dynamic elastic characterization of carbonate rocks used
576 as building materials in the historical city centre of Cagliari (Italy). *Quarterly Journal of*
577 *Engineering Geology & Hydrogeology* 47:259–266
- 578 Cuomo M, Greco L (2018) An implicit strong G^1 -conforming formulation for the analysis
579 of the Kirchhoff plate model. *Continuum Mechanics and Thermodynamics* pp 1–25, DOI
580 10.1007/s00161-018-0701-3
- 581 Di Pasquale S (1996) *The art of construction: between knowledge and science*. Marsilio,
582 Venezia, (in Italian)
- 583 DIANA (2015) *DIANA Finite Element Analysis User's Manual — Release 10.2*. DIANA
584 FEA BV., Delft, <https://dianafea.com/DIANA-manuals>
- 585 Eissa EA, Kazi A (1988) Relation between static and dynamic Young's moduli of rocks. *In-*
586 *ternational Journal of Rock Mechanics and Mining Sciences & Geomechanics Abstracts*
587 25:479–482
- 588 Eremeyev VA, Altenbach H (2017) Basics of mechanics of micropolar shells. In: Al-
589 tenbach H, Eremeyev V (eds) *Shell-like Structures: Advanced Theories and Applications*,
590 Springer, Cham, Switzerland, pp 63–111
- 591 Eremeyev VA, Lebedev LP, Cloud MJ (2015) The Rayleigh and Courant variational princi-
592 ples in the six-parameter shell theory. *Mathematics and Mechanics of Solids* 20:806–822
- 593 Fitchen J (1961) *The construction of gothic cathedrals: a study of medieval vault erection*.
594 University of Chicago Press, Chicago
- 595 Freddi M, Salinas R (1959) The church of S. Maria del Monte in Cagliari. *Bollettino Tecnico*
596 *del Circolo Culturale degli Ingegneri e Architetti Sardi* 12:1–8, (in Italian)

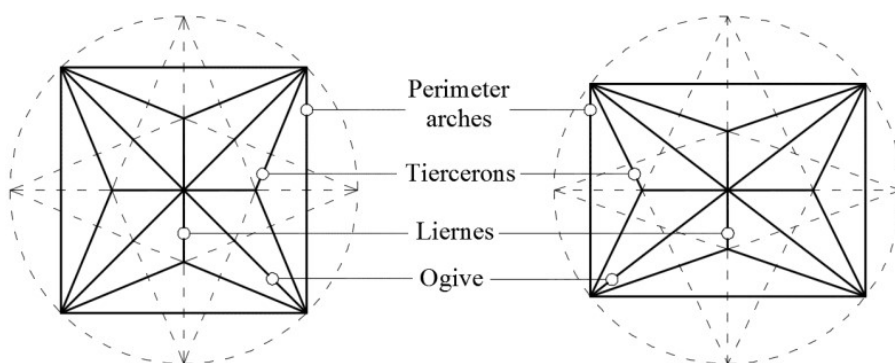
- 597 Gaetani A, Lourenço PB, Monti G, Milani G (2017) A parametric investigation on the seis-
598 mic capacity of masonry cross vaults. *Engineering Structures* 148:686–703
- 599 Garmendia L, Marcos I, Garbin E, Valluzzi MR (2014) Strengthening of masonry arches
600 with textile-reinforced mortar: experimental behaviour and analytical approaches. *Mate-
601 rials and Structures* 47:2067–2080
- 602 Grillanda N, Manconi F, Stochino F, Cazzani A, Bondi F, Chiozzi A, Tralli A (2017) On the
603 analysis of the stellar vault of Santa Maria del Monte in Cagliari. In: *Proceedings of the
604 International Conference of Computational Methods in Sciences and Engineering 2017
605 (ICCMSE-2017)*, Thessaloniki, pp 200008–1–4, DOI 10.1063/1.5012484
- 606 Heyman J (1995) *The stone skeleton: structural engineering of masonry architecture*. Cam-
607 bridge University Press, Cambridge
- 608 Huerta Fernández S (2006) Geometry and equilibrium: The gothic theory of structural de-
609 sign. *The Structural Engineer* 84(2):23–28
- 610 Huerta Fernández S (2009) The debate about the structural behaviour of gothic vaults: From
611 Viollet-le-Duc to Heyman. In: *Proceedings of the Third International Congress on Con-
612 struction History*, Cottbus, vol 2, pp 837–844
- 613 Iannuzzo A, Angelillo M, De Chiara E, De Guglielmo F, De Serio F, Ribera F, Gesualdo A
614 (2018) Modelling the cracks produced by settlements in masonry structures. *Meccanica*
615 53:1857–1873
- 616 Kennicott PR (1996) *Initial Graphics Exchange Specification*,
617 IGES 5.3. U.S. Product Data Association, N. Charleston, SC,
618 <https://books.google.com/books?id=FHPhGwAACAAJ&pgis=1> (accessed June 13,
619 2018)
- 620 Khakalo S, Niiranen J (2017) Isogeometric analysis of higher-order gradient elasticity by
621 user elements of a commercial finite element software. *CAD Computer Aided Design*

- 622 82:154–169
- 623 Kulig A, Romaniak K (2007) Geometrical models of stellar vaults. *Journal of Polish Society*
624 for Geometry and Engineering Graphics 17:51–56
- 625 Lassus JBA (1858) *Album de Villard de Honnecourt, Architecte du XIIIe siècle*. Imprimerie
626 Impériale, Paris
- 627 Lengyel G (2017) Discrete element analysis of gothic masonry vaults for self-weight and
628 horizontal support displacement. *Engineering Structures* 148:195–209
- 629 Manconi F (2015) A static analysis of ribbed groin vaults. The stellar vault of Santa Maria
630 del Monte church. Master’s thesis, University of Cagliari, Italy, (in Italian)
- 631 McNeel R (2008) *Rhinoceros: NURBS modeling for Windows*. Robert McNeel & Asso-
632 ciates, Seattle, <https://books.google.com/books?id=9PjVZwEACAAJ&pgis=1> (accessed
633 June 13, 2018)
- 634 Milani G, Taliercio A (2016) Limit analysis of transversally loaded masonry walls using an
635 innovative macroscopic strength criterion. *International Journal of Solids and Structures*
636 81:274–293
- 637 Milani G, Lourenço PB, Tralli A (2006) Homogenised limit analysis of masonry walls, Part
638 I: Failure surfaces. *Computers & Structures* 84:166–180
- 639 Milani G, Simoni M, Tralli A (2014) Advanced numerical models for the analysis of ma-
640 sonry cross vaults: A case-study in Italy. *Engineering Structures* 76:339–358
- 641 Miśkiewicz M (2018) Structural response of existing spatial truss roof construction based
642 on cosserat rod theory. *Continuum Mechanics and Thermodynamics* pp 1–21, DOI
643 10.1007/s00161-018-0660-8
- 644 NTC 2008 (2008) *Technical Rules for Constructions (Italian Building Code)*. *Gazzetta Uf-*
645 *ficiale* n. 29. February 4, 2008 - Suppl. Ordinario n. 30, (in Italian)

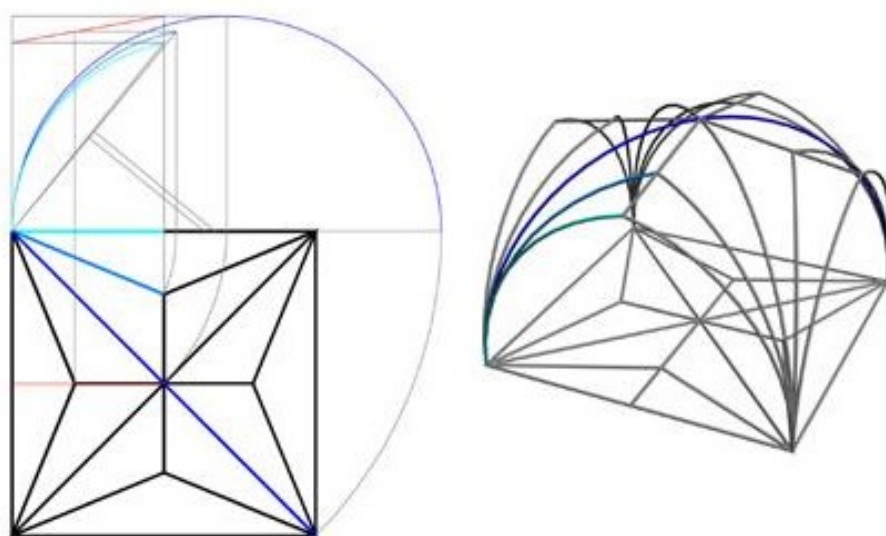
- 646 Parisi F, Augenti N (2012) A shear response surface for the characterization of unit mortar
647 interfaces. In: 15th IB2MaC, International Brick and Block Masonry Conference, Flo-
648 rianópolis, Brazil
- 649 Piegler L, Tiller W (1995) The NURBS book. Springer, Berlin-Heidelberg
- 650 Placidi L, Greco L, Bucci S, Turco E, Rizzi NL (2016) A second gradient formulation for
651 a 2D fabric sheet with inextensible fibres. *Zeitschrift für Angewandte Mathematik und*
652 *Physik (ZAMP)* 67:#114–1–24
- 653 Placidi L, Barchiesi E, Misra A (2018) A strain gradient variational approach to damage: a
654 comparison with damage gradient models and numerical results. *Mathematics and Me-*
655 *chanics of Complex Systems* 6:77–100
- 656 Ramaglia G, Lignola GP, Prota A (2016) Collapse analysis of slender masonry barrel vaults.
657 *Engineering Structures* 117:86–100
- 658 Sabouret V (1928) Les voûtes d'arêtes nervurées. Rôle simplement décoratif des nervures.
659 *Le Génie Civil* 92:205–209
- 660 Sturm JF (1999) Using SeDuMi 1.02, a MATLAB toolbox for optimization over symmetric
661 cones. *Optimization Methods and Software* 11:625–653
- 662 Ther T, Sajtos I, Armuth M, Strommer L (2010) Ribbed vaults of the Nagyvázsony
663 monastery church — Geometrical factor of safety highlights the secret. *Periodica Poly-*
664 *technica Architecture* 41:3–8
- 665 Turco E (2018) Discrete is it enough? The revival of Piola-Hencky keynotes to analyze
666 three-dimensional Elastica. *Continuum Mechanics and Thermodynamics* pp 1–19, DOI
667 10.1007/s00161-018-0656-4
- 668 Ungewitter G, Mohrmann K (1890) *Lehrbuch der gotischen Konstruktionen*, 4th edn. Tauch-
669 nitz, Leipzig

- 670 Valluzzi MR (2007) On the vulnerability of historical masonry structures: analysis and mit-
671 igation. *Materials and Structures* 40:723–743
- 672 Viollet-le-Duc EE (1854–1868) *Dictionnaire raisonné de l’architecture française du XIe au*
673 *XVIe siècle*, vol 1–9. Bance—Morel, Paris
- 674 Willis R (1842) On the construction of the vaults of the Middle Ages. *Transactions of the*
675 *Royal Institute of British Architects* 1:1–69
- 676 Yildizdag ME, Demirtas M, Ergin A (2018) Multipatch discontinuous galerkin isogeometric
677 analysis of composite laminates. *Continuum Mechanics and Thermodynamics* pp 1–14,
678 DOI 10.1007/s00161-018-0696-9

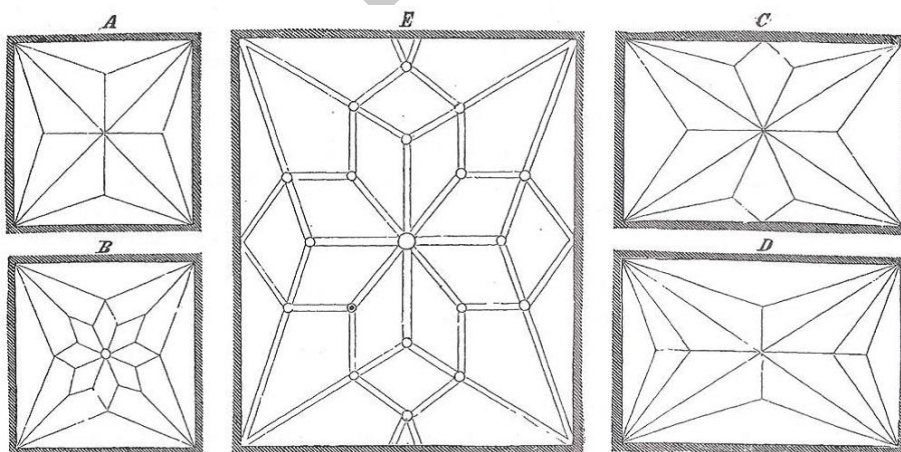
Pre-Print



(a) Projection of the rib-system on the horizontal plane



(b) Graphic method for construction



(c) Some different stellar vaults' patterns

Please cite this document as: N. Grillanda, A. Chiozzi, F. Bondi, A. Tralli, F. Manconi, F. Biondi and A. Casini "Numerical insights on the structural assessment of historical masonry stellar vaults: the case of Santa Maria del Monte in Cagliari" *Continuum Mechanics and Thermodynamics*, Vol 33:1–24, 2021. DOI:10.1007/s00161-019-00752-8

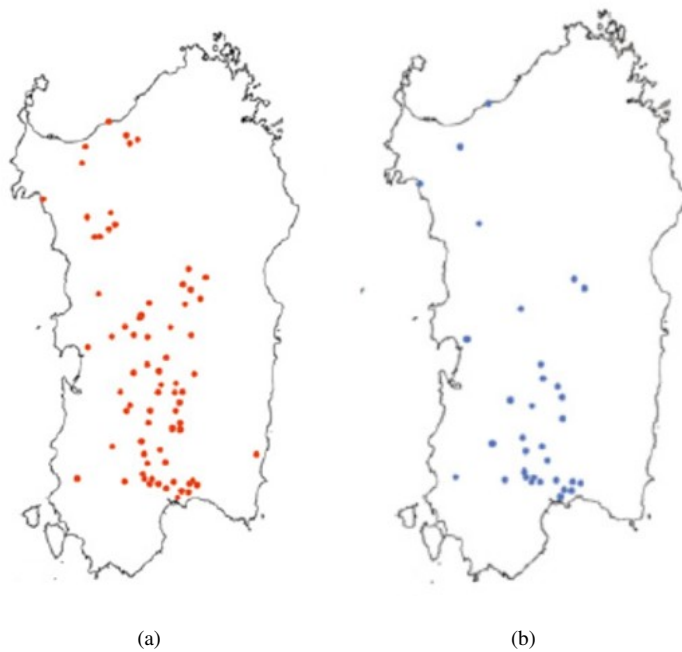


Fig. 2 Distribution of late-Gothic vaults in Sardinia: ribbed vaults (a) and stellar vaults (b). The image has been graphically elaborated from that originally presented in (Casu, 2013).

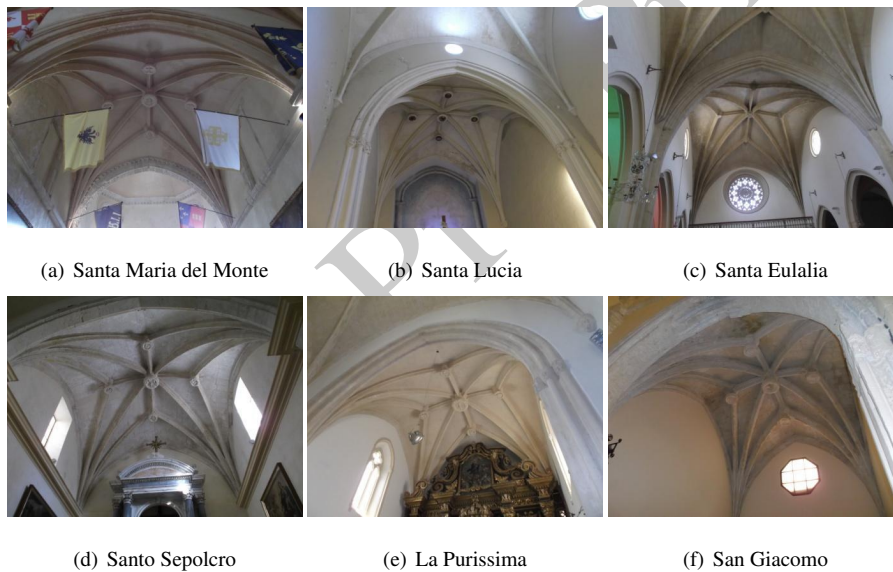


Fig. 3 Stellar vaults built in some churches located in Cagliari.

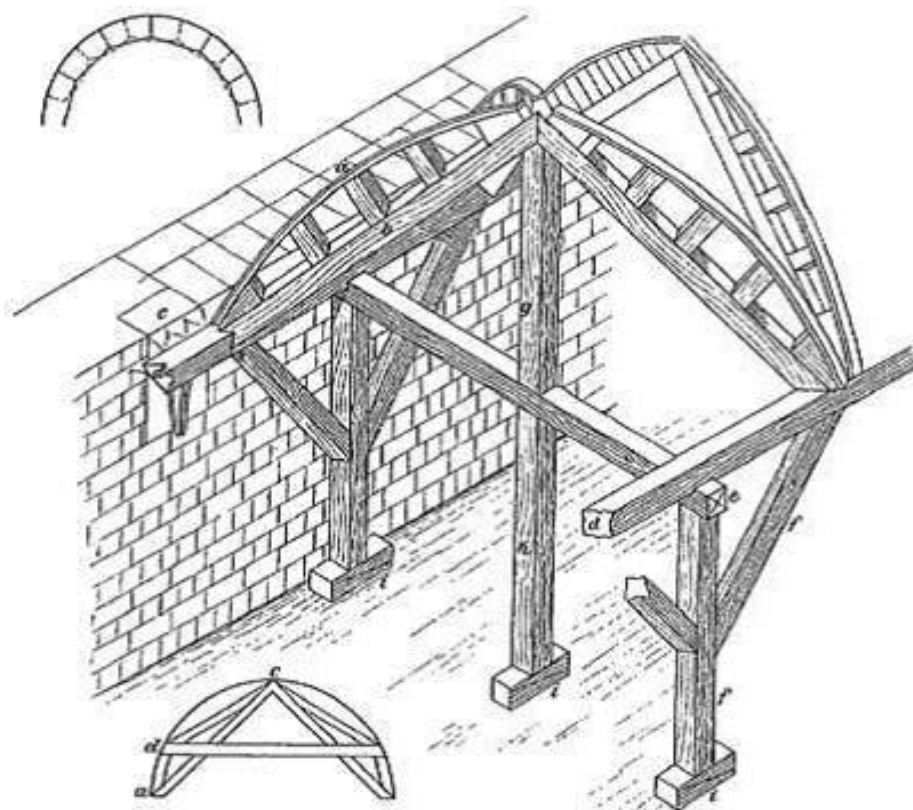


Fig. 4 Building system for Gothic ribbed vaults using centrings for the preliminary construction of ribs.

Image elaborated from (Ungewitter and Mohrmann, 1890).

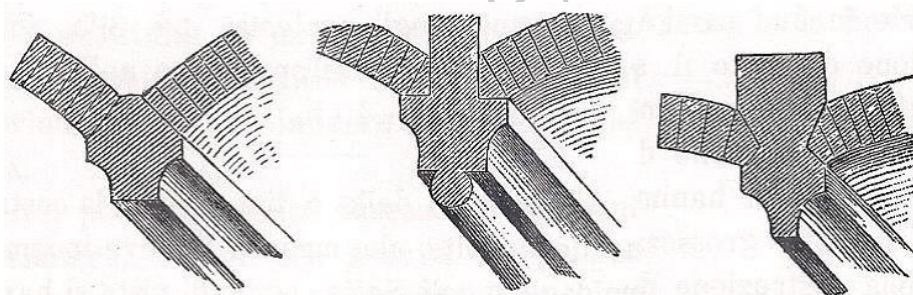


Fig. 5 Some examples of connections between diagonal ribs and vaults. Image elaborated from (Ungewitter and Mohrmann, 1890).

Please cite this document as: N. Grillanda, A. Chiozzi, F. Bondi, A. Tralli, F. Manconi, F. Stochino and A. Cazzani "Numerical insights on the structural assessment of historical masonry stellar vaults: the case of Santa Maria del Monte in Cagliari" Continuum Mechanics and Thermodynamics, Vol 33:1–24, 2021. DOI:10.1007/s00161-019-00752-8



Fig. 6 Facade of the church of Santa Maria del Monte.

Please cite this document as: N. Grillanda, A. Chiozzi, F. Bondi, A. Tralli, F. Manconi, F. Stochino and A. Cazzani "Numerical insights on the structural assessment of historical masonry stellar vaults: the case of Santa Maria del Monte in Cagliari" Continuum Mechanics and Thermodynamics, Vol 33:1–24, 2021. DOI:10.1007/s00161-019-00752-8



(a) Stellar vault located at the presbytery (b) Geometric outline of the vault obtained by laser scanning techniques

Fig. 7 Santa Maria del Monte stellar vault.

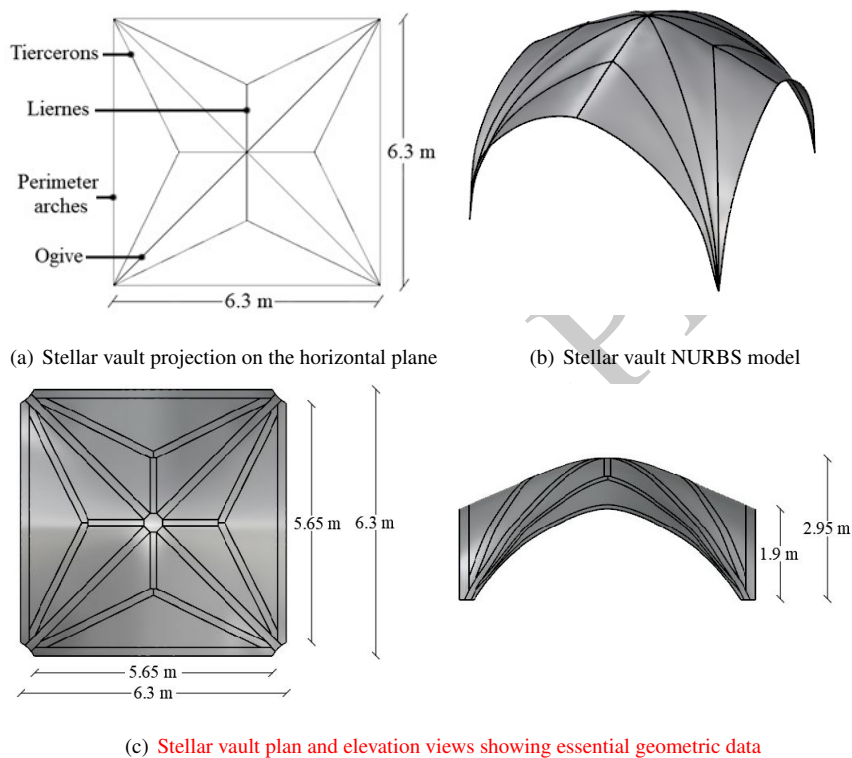


Fig. 8 Geometric model of the vault: essential geometric data are reported.

Please cite this document as: N. Grillanda, A. Chiozzi, F. Bondi, A. Tralli, F. Manconi, F. Stochino and A. Cazzani "Numerical insights on the structural assessment of historical masonry stellar vaults: the case of Santa Maria del Monte in Cagliari" *Continuum Mechanics and Thermodynamics*, Vol 33:1–24, 2021. DOI:10.1007/s00161-019-00752-8

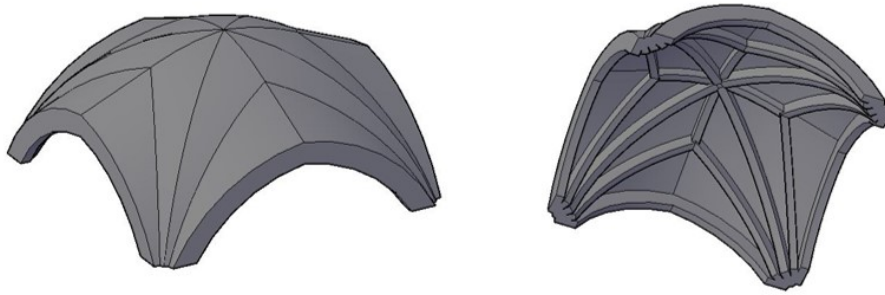


Fig. 9 3D CAD model of the vault: extrados (left) and intrados (right).

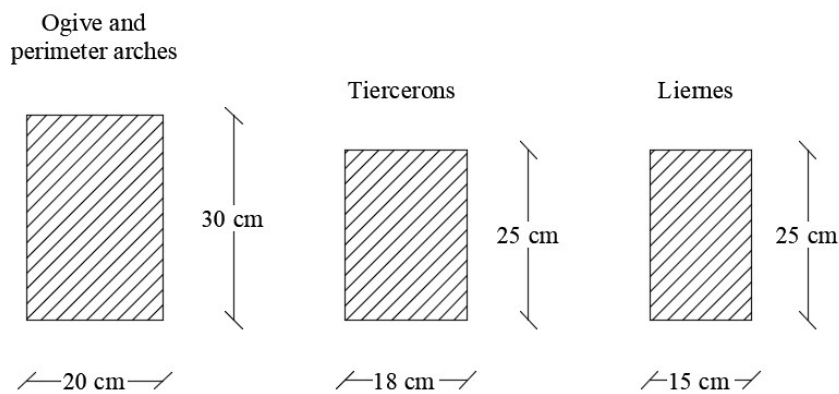


Fig. 10 Simplified cross-sections assumed for modeling ribs.

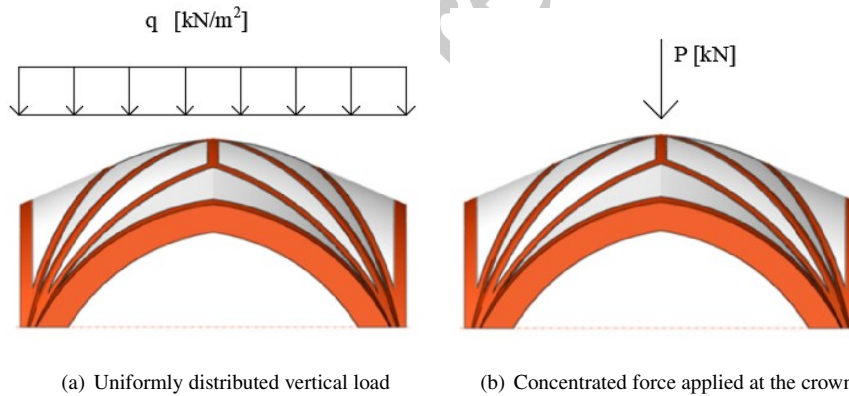


Fig. 11 Considered load conditions.

Please cite this document as: N. Grillanda, A. Chiozzi, F. Bondi, A. Tralli, F. Manconi, F. Stochino and A. Cazzani "Numerical insights on the structural assessment of historical masonry stellar vaults: the case of Santa Maria del Monte in Cagliari" *Continuum Mechanics and Thermodynamics*, Vol 33:1–24, 2021. DOI:10.1007/s00161-019-00752-8

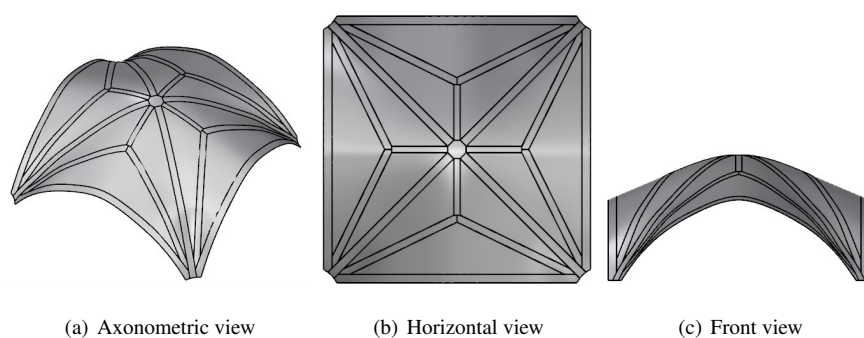


Fig. 12 NURBS model in Rhinoceros®.

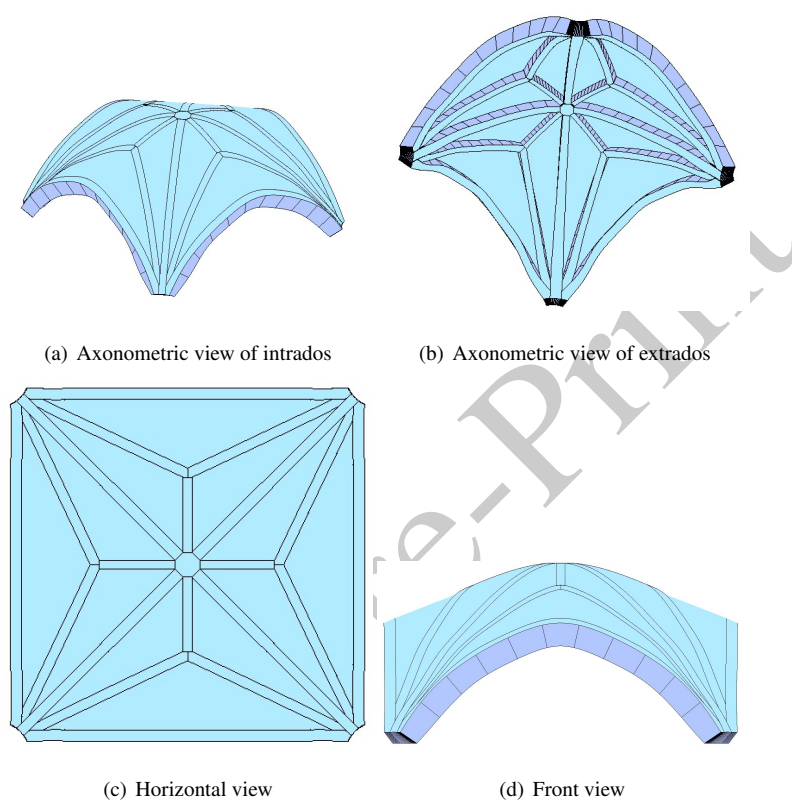
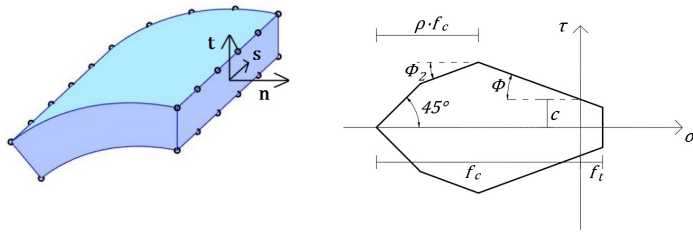
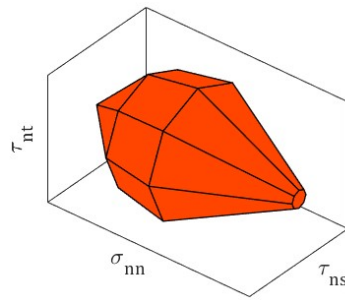


Fig. 13 NURBS model in MATLAB.



(a) Masonry-masonry interface and corresponding local reference system (b) Parameters of the failure surface



(c) Adopted 3D linearized failure surface

Fig. 14 Masonry collapse criterion.

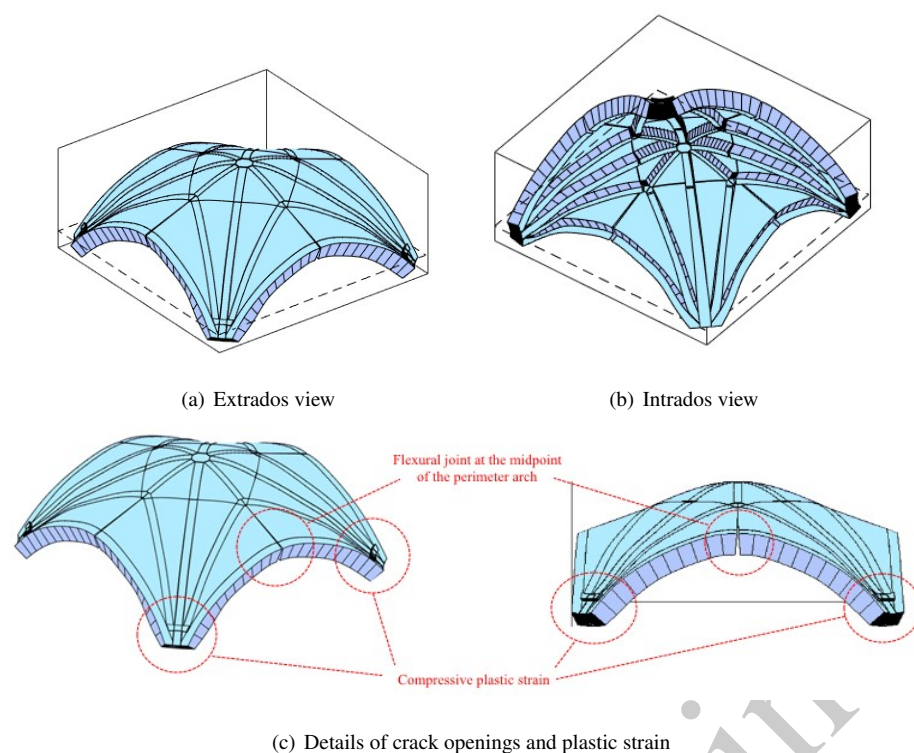


Fig. 15 Collapse mechanism associated with the uniformly distributed load.

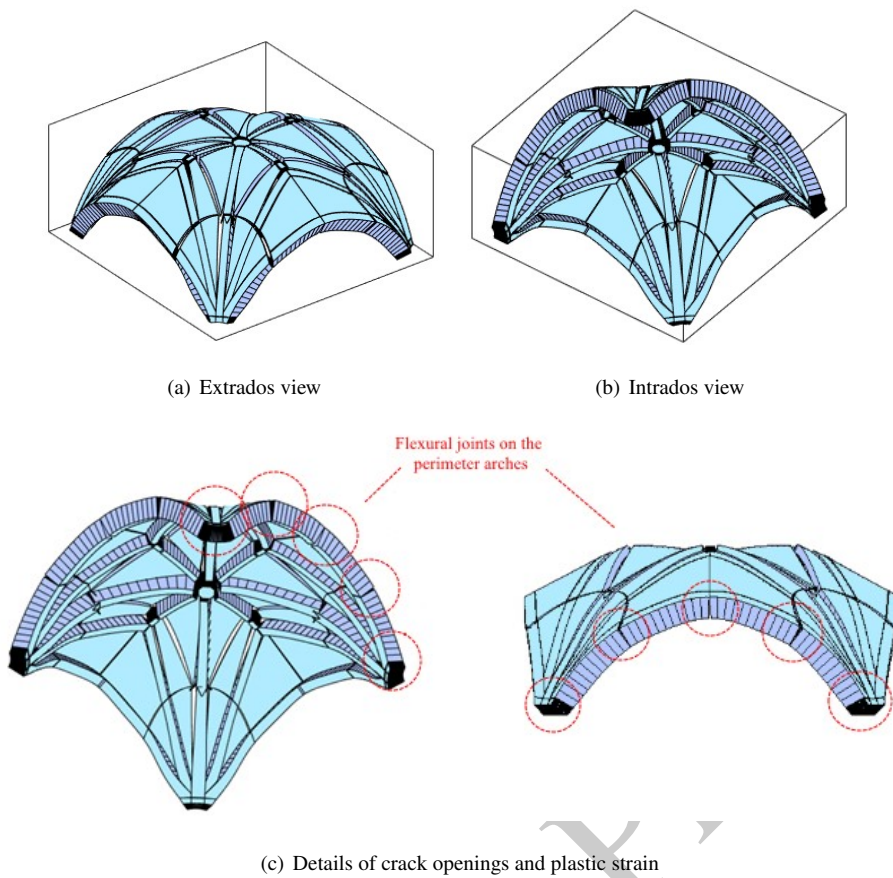


Fig. 16 Collapse mechanism associated with the vertical point load applied at the crown.

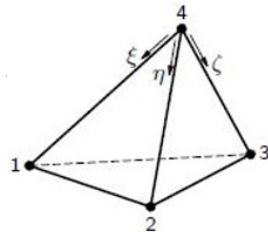


Fig. 17 Tetrahedral finite element (TE12L in DIANA) and corresponding degrees of freedom per node (DIANA, 2015).

Please cite this document as: N. Grillanda, A. Chiozzi, F. Bondi, A. Tralli, F. Manconi, F. Stochino and A. Cazzani "Numerical insights on the structural assessment of historical masonry stellar vaults: the case of Santa Maria del Monte in Cagliari" *Continuum Mechanics and Thermodynamics*, Vol 33:1–24, 2021. DOI:10.1007/s00161-019-00752-8

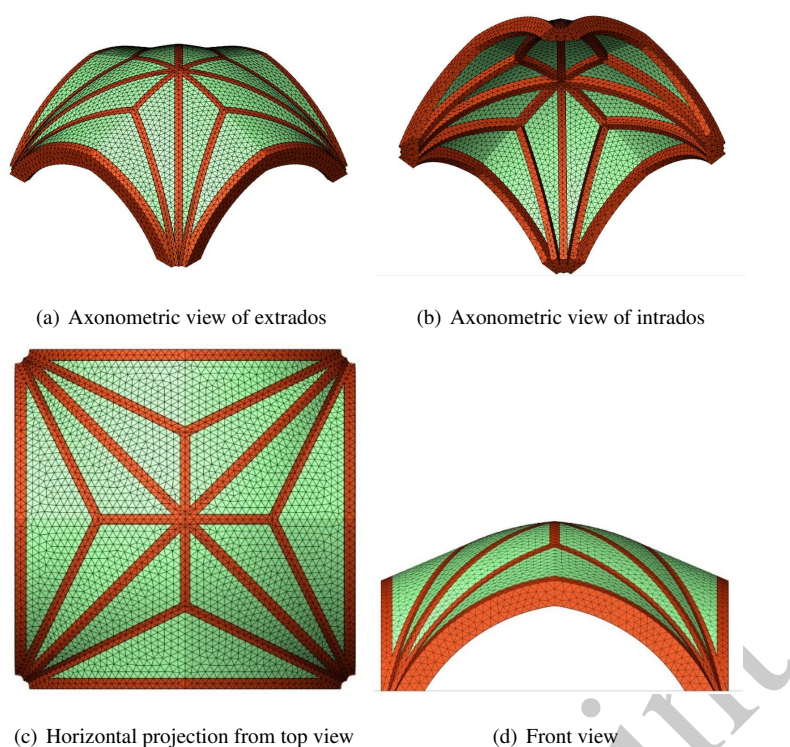


Fig. 18 FEM model in DIANA.

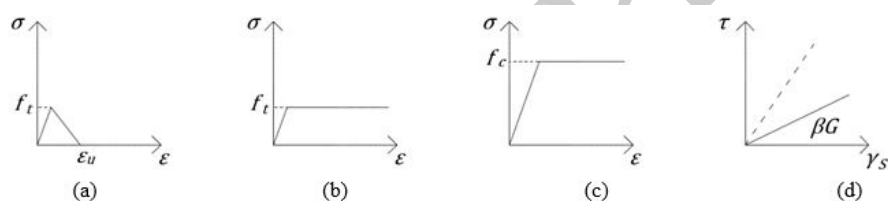


Fig. 19 Non-linear masonry behavior selected in TSCM, (a) bilinear elastic-softening tensile behavior, (b) Elastic-plastic tensile behavior, (c) Elastic-plastic compression behavior, (d) Linear shear behavior with reduced stiffness.

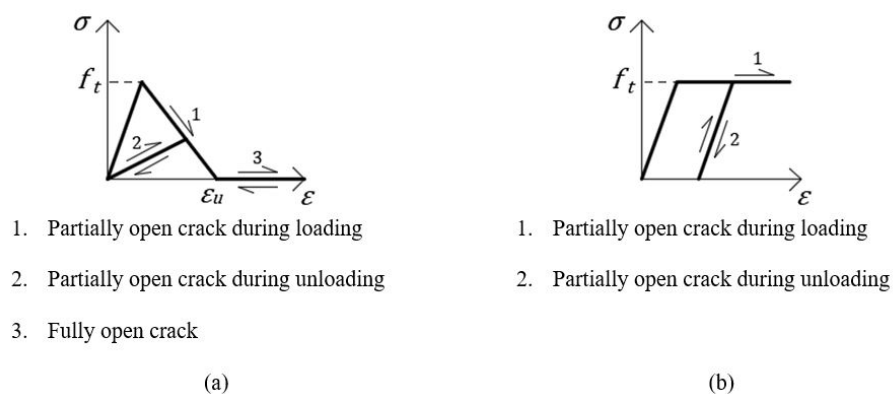


Fig. 20 Different type of damage for each branch of the two adopted tensile behaviors: (a) bilinear elastic-softening behavior, (b) elastic-plastic behavior.

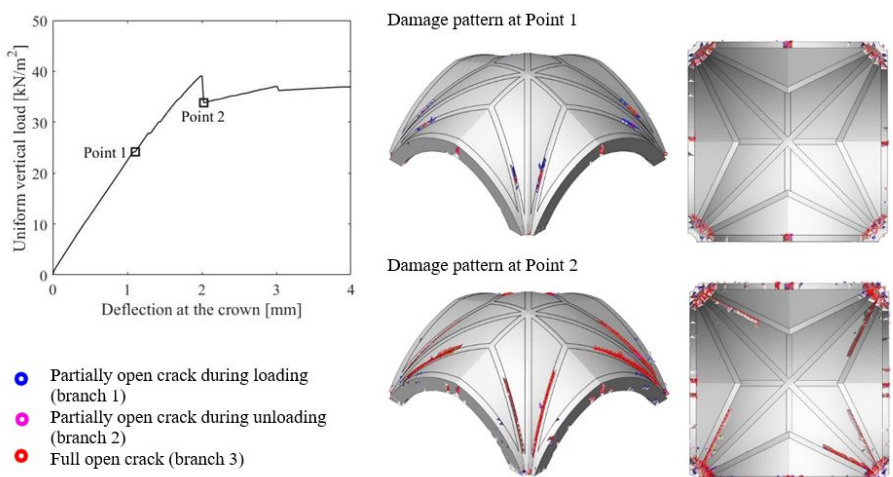


Fig. 21 Results of non-linear static analysis under uniformly distributed vertical load with a bilinear behavior in tension: load-deflection diagram and resulting crack patterns (axonometric and intrados views) at the load level marked by Point 1 and Point 2.

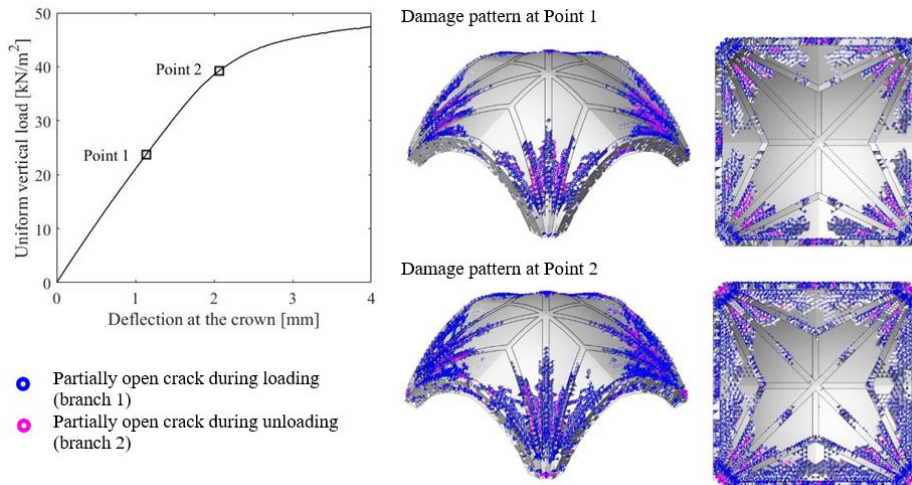


Fig. 22 Results of non-linear static analysis under uniformly distributed vertical load with an elastic-plastic behavior in tension: load-deflection diagram and resulting crack patterns (axonometric and intrados views) at the load level marked by Point 1 and Point 2.

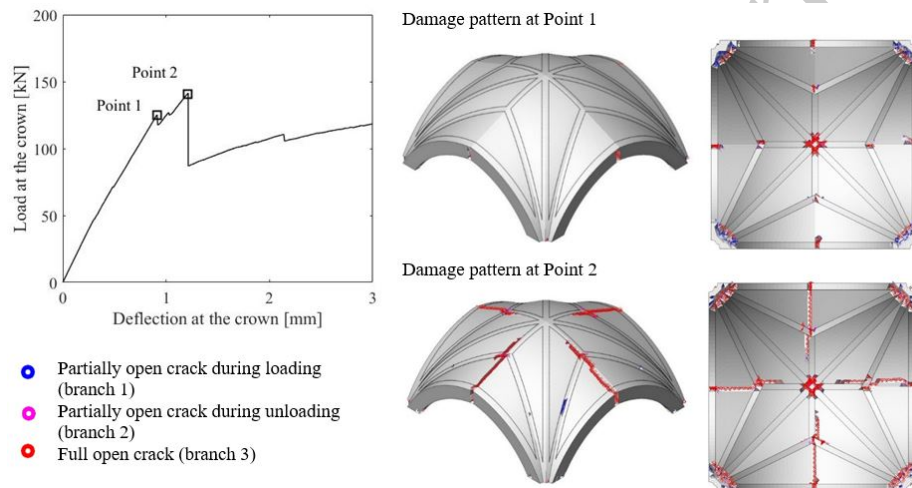


Fig. 23 Results of non-linear static analysis under concentrated load applied at the crown, with a bilinear behavior in tension: load-deflection diagram and resulting crack patterns (axonometric and intrados views) at the load level marked by Point 1 and Point 2 in the load-deflection curve.

Please cite this document as: N. Grillanda, A. Chiozzi, F. Bondi, A. Tralli, F. Manconi, F. Stochino and A. Cazzani "Numerical insights on the structural assessment of historical masonry stellar vaults: the case of Santa Maria del Monte in Cagliari" *Continuum Mechanics and Thermodynamics*, Vol 33:1–24, 2021. DOI:10.1007/s00161-019-00752-8

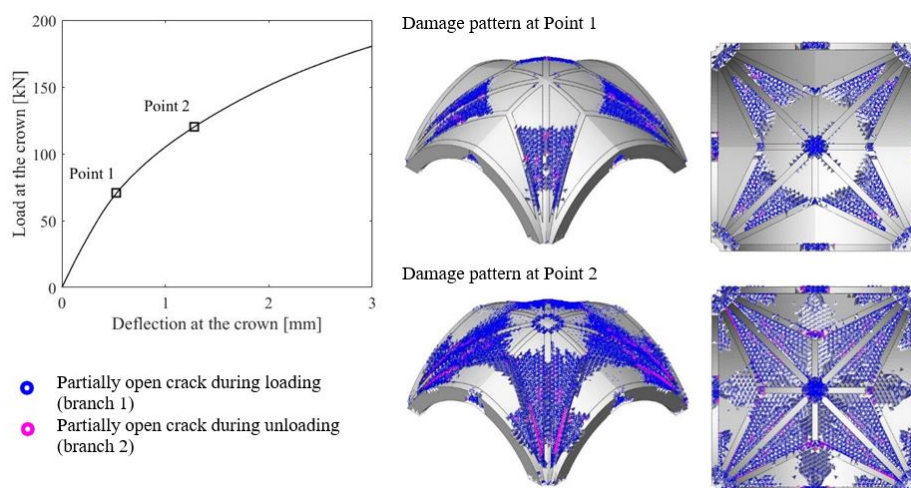


Fig. 24 Results of non-linear static analysis under concentrated load applied at the crown with an elastic-plastic behavior in tension: load-deflection diagram and resulting crack patterns (axonometric and intrados views) at the load level marked by Point 1 and Point 2.

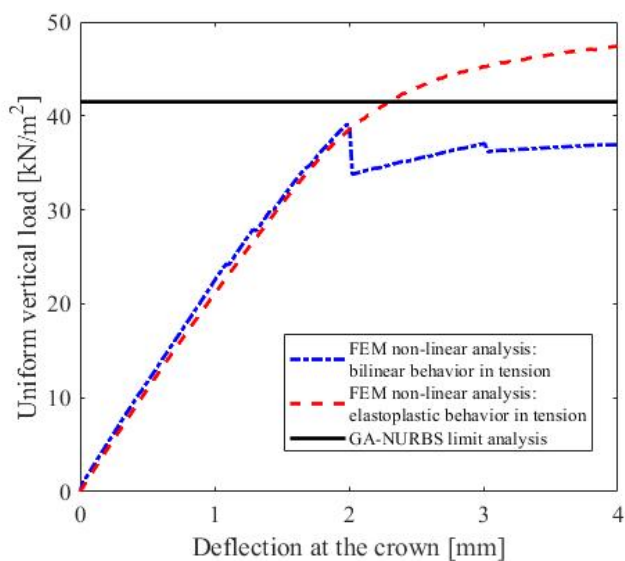


Fig. 25 Analyses with uniformly distributed vertical load: comparison of load-deflection results between FEM and limit analysis based on GA-NURBS modeling.

Please cite this document as: N. Grillanda, A. Chiozzi, F. Bondi, A. Tralli, F. Manconi, F. Stochino and A. Cazzani "Numerical insights on the structural assessment of historical masonry stellar vaults: the case of Santa Maria del Monte in Cagliari" *Continuum Mechanics and Thermodynamics*, Vol 33:1–24, 2021. DOI:10.1007/s00161-019-00752-8

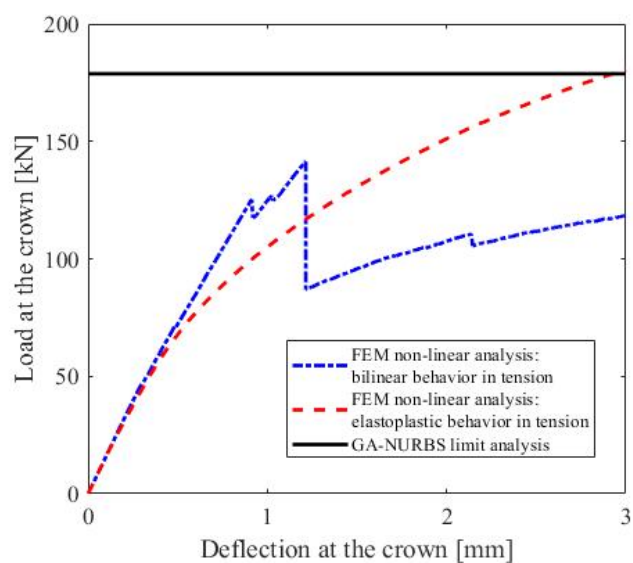


Fig. 26 Analyses with concentrated point force applied at the crown: comparison of load-deflection results between FEM and limit analysis based on GA-NURBS modeling.

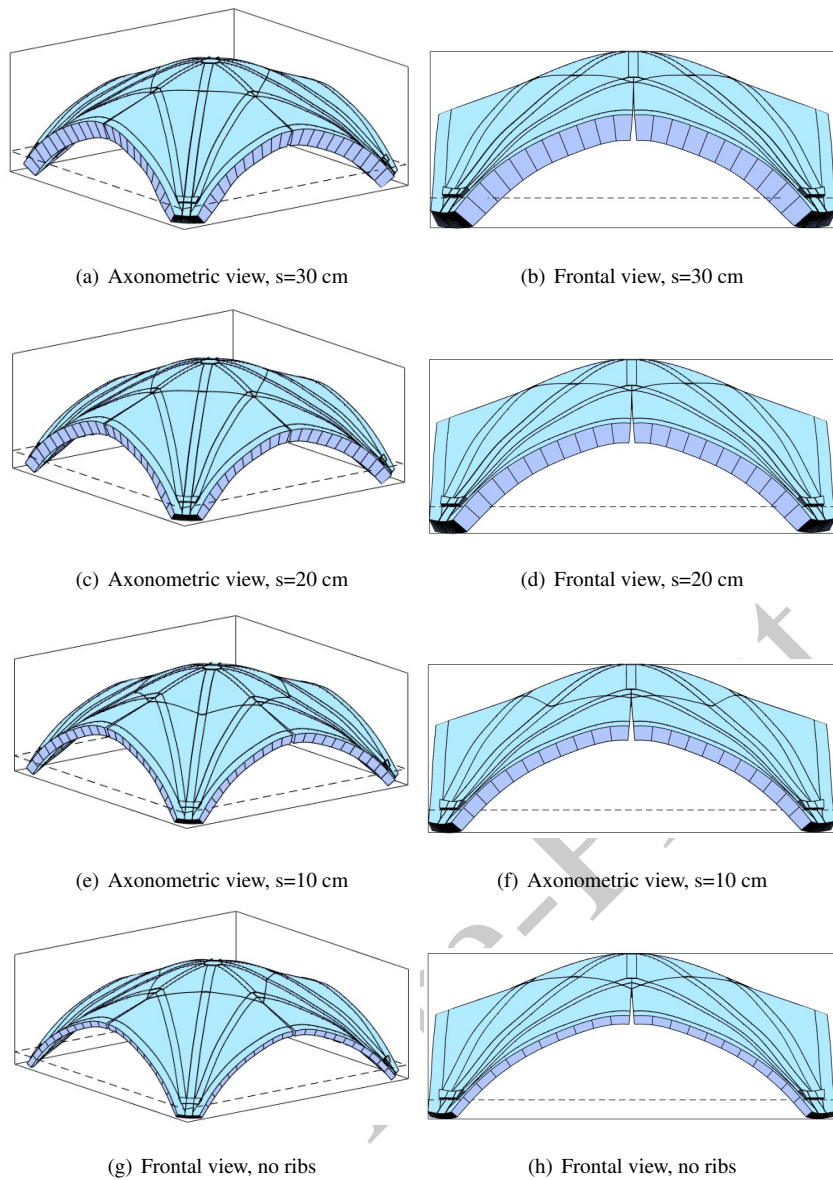


Fig. 27 Detected collapse mechanisms for some values of rib thickness (axonometric view on the left and front view on the right).

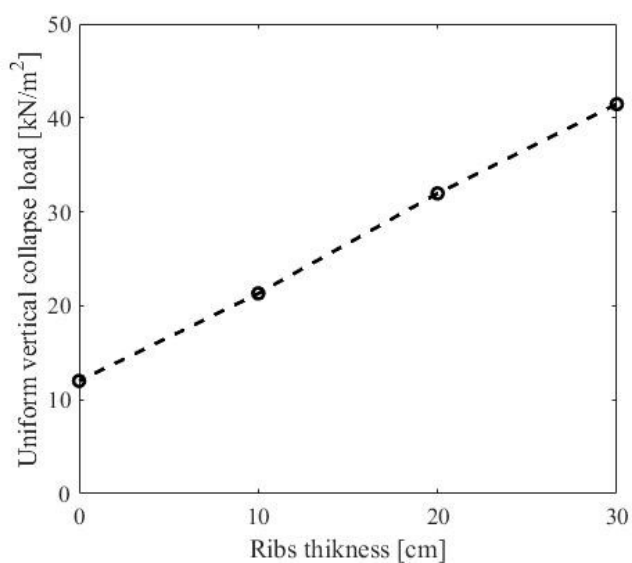


Fig. 28 Collapse load as a function of ribs thickness for the case of uniformly distributed vertical load.